Rapid Communications

Semiquantum thermodynamics of complex ferrimagnets

Joseph Barker[1] and Gerrit E. W. Bauer[2,3]

[1]*Institute for Materials Research, Tohoku University, Sendai 980-8577, Japan*

[2]*Institute for Materials Research & AIMR & CSRN, Tohoku University, Sendai 980-8577, Japan*

[3]*Zernike Institute for Advanced Materials, University of Groningen, 9747 AG Groningen, The Netherlands*

(Received 1 February 2019; revised manuscript received 11 July 2019; published 2 October 2019)

High-quality magnets such as yttrium iron garnet (YIG) are electrically insulating and very complex. By implementing a quantum thermostat into atomistic spin dynamics we compute YIG's key thermodynamic properties, viz., the magnon power spectrum and specific heat, for a large temperature range. The results differ (sometimes spectacularly) from simple models and classical statistics, but agree with available experimental data.

DOI: 10.1103/PhysRevB.100.140401

Introduction. The spin dynamics of electrically insulating magnets often has high quality because the dissipation channel by conduction electron scattering is absent. With few exceptions, they are complex ferrimagnets. Yttrium iron garnet (YIG) with 80 atoms in the unit cell rules with a record low Gilbert damping of long-wavelength spin-wave excitations or magnons, even at room temperature [1,2]. The implied exceptionally low disorder and weak coupling with phonons remains a mystery, however. Recently, magnon heat and spin transport were measured in YIG thin films in a nonlocal spin injection and detection configuration with Pt contacts by means of the spin Hall effect [3] and modeled by spin diffusion [4]. Key parameters of this model are linked to the thermodynamics of the magnetic order, such as the magnon heat capacity, which is difficult to measure because it is orders of magnitude smaller than the phonon heat capacity—at 10 K the magnon and phonon heat capacities are $C_m \approx 0.009$ J kg^{-1} K^{-1} and $C_p \approx 0.270$ J kg^{-1} K^{-1} [5]. They can be separated by magnetic freeze-out of the magnon contribution at temperatures up to a few degrees Kelvin [5,6]. The magnon heat capacity at higher temperatures has been estimated by extrapolating models that agree with experimental low-temperature results [4,7]. YIG is often treated as a single-mode ferromagnet with quadratic $\omega \propto \mathcal{D}k^2$ (or isotropic cosine function) dispersion, thereby ignoring higher-frequency acoustic and optical modes and the temperature dependence of the exchange stiffness $\mathcal{D}$. Furthermore, magnon-magnon interactions are also commonly neglected or treated in a mean-field approximation. Statistical approaches also have issues, such as the use of classical (Johnson-Nyquist) thermal noise at low temperatures [8].

In this Rapid Communication we introduce a numerical method that avoids all of these shortcomings. It allows us to carry out material-dependent thermodynamic calculations that are quantitatively accurate with a small number of parameters that can be determined independently. The crucial ingredient is a thermostat for Planck quantum (rather than Rayleigh-Jeans classical) statistics in an atomistic spin dynamics framework [9].

With the inclusion of quantum thermal statistics we find quantitative agreement for YIG with available experiments at low temperatures. The computed spin-wave dispersion as a function of temperature agrees well with results from neutron scattering. This low-temperature quantitative benchmarking imbues trust in the technique for calculating thermodynamic functions and allows access to quantities such as the magnon heat capacity at room temperature that turns out to be an order of magnitude larger than previous estimates.

Method. We address the thermodynamics by computing the atomistic spin dynamics in the long (ergodic) time limit to generate canonical ensembles of spins. The magnetic moments ("spins") in this model are treated as classical unit vectors $\mathbf{S}$, an excellent approximation for the half-filled $3d$ shell of the iron cations in YIG with $\mathcal{S} = 5/2$ and magnetic moment $\mu_s = g\mu_B\mathcal{S}$, where $g \approx 2$ is the electron g-factor and μ_B the Bohr magneton.

The Heisenberg Hamiltonian $\mathscr{H} = -\frac{1}{2}\sum_{ij} J_{ij}\mathbf{S}_i \cdot \mathbf{S}_j$ contains the (super)exchange parameters J_{ij} between spins on sites i and j, which are determined by fits to inelastic neutron scattering data [10]. Recently, the magnon dispersions were measured again with a higher resolution [11], allowing an improved parametrization of the six nearest-neighbor exchange constants, which we adopt in the following. We add a Zeeman term, $\mathscr{H} = -\sum_i \mu_{s,i}\mathbf{H}_{\text{ext}} \cdot \mathbf{S}_i$ with $\mathbf{H}_{\text{ext}} = H_z = 0.1$ T, to fix the quantization axis. On each lattice site "i" the spin dynamics obey the Landau-Lifshitz equation of motion [12],

$$\frac{\partial \mathbf{S}_i}{\partial t} = -|\gamma|[\mathbf{S}_i \times \mathbf{H}_i + \eta\mathbf{S}_i \times (\mathbf{S}_i \times \mathbf{H}_i)], \tag{1}$$

where $\gamma = g\mu_B/\hbar$ is the gyromagnetic ratio and η is a damping constant. Each spin feels an effective magnetic field $\mathbf{H}_i = \boldsymbol{\xi}_i - (1/\mu_{s,i})\partial\mathscr{H}/\partial\mathbf{S}_i$, where $\boldsymbol{\xi}_i$ are stochastic processes controlled by the thermostat at temperature T. $\langle\xi_{i\alpha}\rangle = 0$ and the correlation function in frequency space is governed by the fluctuation-dissipation theorem (FDT) $\langle\xi_{i\alpha}\xi_{j\beta}\rangle_\omega = 2\eta\delta_{ij}\delta_{\alpha\beta}\varphi(\omega, T)/\mu_{s,i}$, where the Kronecker δ's reflect the assumption that the fluctuations between lattice sites i, j and Cartesian coordinates α, β are uncorrelated. $\varphi(\omega, T)$ describes the temperature dependence of the noise power and is chosen such that the steady-state distribution functions obey equilibrium thermal statistics. By not approximating the spin

Hamiltonian by a truncated Holstein-Primakoff expansion, our approach includes magnon-magnon interactions to all orders [13].

Atomistic spin dynamics methods generally assume the classical limit of the FDT with frequency-independent (white) noise $\varphi(\omega, T) = k_B T$, i.e., *all* magnons are stimulated. The energy equipartition of the coupled system results in the Rayleigh-Jeans magnon distribution. However, this is only valid when the thermal energy is much larger than that of the magnon mode k under consideration, i.e., when $k_B T \gg \hbar\omega_k$, while the energies of the YIG magnon spectrum—and that of most room-temperature magnets—extend up to $\hbar\omega_{\mathbf{k}}/k_B \approx$ 1000 K [1]. A classical thermostat therefore generates too many high-energy magnons, which, for example, overestimates the broadening by magnon scattering and leads to other predictions that can be very wrong.

According to the quantum FDT for magnons [14,15],

$$\varphi(\omega, T) = \frac{\hbar\omega}{\exp(\hbar\omega/k_B T) - 1}, \tag{2}$$

which means that equipartition is replaced by Planck statistics of the magnons at temperature T. Quantum statistics in classical spin systems can partially be mimicked through a postprocess rescaling of the temperature [16] or by using temperature-dependent frequencies that rely on analytic expressions for the low-temperature spectrum [15]. These approaches cannot be used to evaluate all thermodynamic properties and are not suitable to treat complex magnets such as YIG. We therefore adopt here the "quantum thermostat" introduced earlier in molecular dynamics [17,18], i.e., a correlated noise source that obeys the quantum FDT. This is "colored" noise, but very different from the one used to describe classical memory effects in the heat bath [19,20].

We implement the quantum statistics by generating correlated fluctuating fields $\boldsymbol{\xi}_i(t)$ numerically in time that obey the FDT in the frequency domain. Savin *et al.* [18] employ a set of stochastic differential equations that produce the required distribution function. We adjust this method to spin dynamics problems, referring the reader to Ref. [18] and the Supplemental Material S1 for the technical details [21]. The solution is a dimensionless stochastic process $\Phi_{i\alpha}(t)$ with the spectrum of Eq. (2). The dimensionful noise in the spin dynamics reads

$$\xi_{i\alpha}(t) = k_B T \sqrt{\frac{2\eta\mu_{s,i}}{\gamma\hbar}}\,\Phi_{i\alpha}(t). \tag{3}$$

When we agitate the model of classical spins with these stochastic fields, the excitations of the ground state (magnons) obey quantum statistics, quite analogous to quantized phonons in a classical ball-spring lattice. This approach may loosely be called "semiquantum" and works very well for the large Fe^{3+} spin in YIG with $\mathcal{S} = 5/2$ ($\mu_s = 5\mu_B$), but requires more scrutiny for spin $\mathcal{S} = 1/2$ (see Supplemental Material S2 [21]).

We integrate Eq. (1) using the Heun method with a time step $\Delta t = 0.1$ fs. The stochastic differential equations of the thermostat are integrated using the fourth-order Runge-Kutta method with the same time step. The exchange parameters from Ref. [11]—scaled by $\mathcal{S}^2$ for to unit spins—

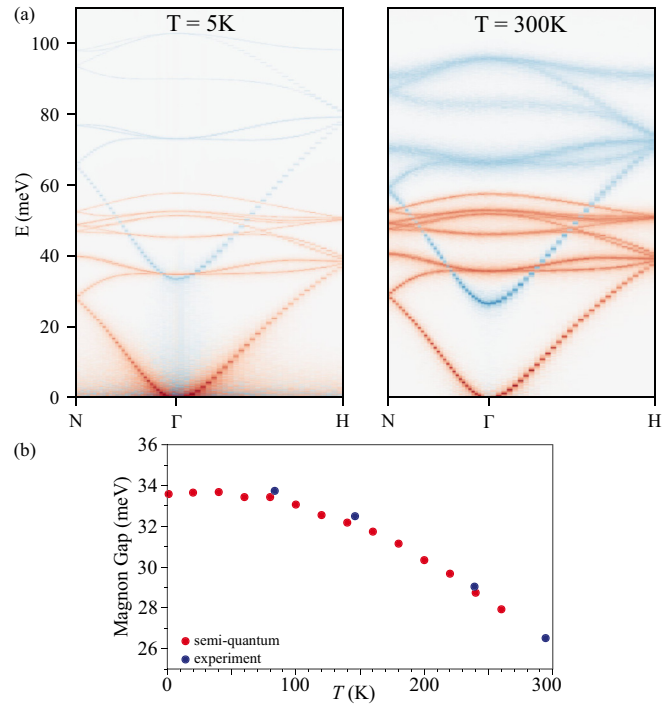

FIG. 1. (a) YIG magnon spectrum at $T = 5$ K and $T = 300$ K calculated using the quantum thermostat and the exchange parameters of Ref. [11]. The color intensity is adjusted on a log scale such that all modes are visible (even for extremely low occupation) and is different for both figures. The red/blue color shows the $+/-$ polarization of the magnons. (b) Magnon gap between optical and acoustic modes at Γ. Experimental data are adopted from neutron scattering experiments [10].

read $J_1 = -42.5$, $J_2 = -3.25$, $J_{3a} = 0$, $J_{3b} = -6.875$, $J_4 = 0.4375$, $J_5 = -2.9375$, $J_6 = 0.5625$ meV for successive nearest neighbors. For the magnon spectrum we use $\eta = 2 \times 10^{-4}$ representing the low Gilbert damping of YIG. For thermodynamic calculations we use overdamped dynamics with $\eta = 0.1$ for faster convergence. Thermodynamic quantities (energy, magnetization) were calculated for 5 ns, discarding the initial equilibration period (generally below 0.1 ns). The remaining time series are used to calculate the thermodynamic averages. Five independent stochastic trajectories were calculated and averaged for each data point. Error bars defined as three times the standard deviation for thermodynamic averages between these trajectories were mostly smaller than the data points in the figures.

Magnon spectrum. We compare now the magnon spectrum computed with the quantum thermostat with our previous work with classical statistics (and older exchange constants from Ref. [1]) [9]. Results for low (5 K) and room (300 K) temperature are shown in Fig. 1(a). The classical thermostat overestimates the number of high-energy magnons and therefore the broadening of the optical modes at higher temperatures. With quantum statistics, the high-energy optical modes are well resolved at room temperature and should be observable by inelastic neutron scattering with large frequency transfer. The agreement between the calculated and measured [10] temperature dependence of the exchange gap between

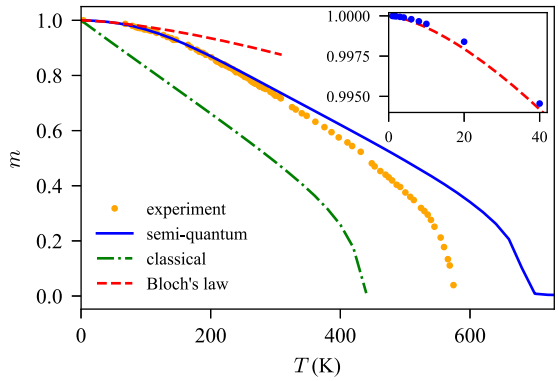

FIG. 2. Temperature-dependent magnetization of YIG calculated using classical and semiquantum spin dynamics. The experimental points are from Ref. [27] and Bloch's law from Eq. (4) with $\mathcal{D} = 85.2 \times 10^{-41}$ J m^2 [11], which in YIG is temperature independent until close to the Curie temperature. The inset is a closeup of the semiquantum method (blue circles) in the low-temperature regime where Bloch's law (dashed red line) is valid.

optical and acoustic modes at the Γ point, shown in Fig. 1(b), is improved, especially in the low-temperature regime.

Magnetization. The magnetization at low temperatures $m_z = 1 - \frac{1}{\mathcal{S}} \sum_{\mathbf{k}\nu} \langle n_{\mathbf{k}\nu} \rangle_T$, where $\langle n_{\mathbf{k}\nu} \rangle_T$ is the distribution of magnons with wave vector $\mathbf{k}$ and band index ν in the first Brillouin zone, cannot be calculated correctly with classical statistics [22] (at higher temperatures the expression does not hold since magnon-magnon interactions are important). This is obvious already for the single parabolic band, noninteracting magnon gas model for which

$$1 - m_z(T) = v_{\mathrm{ws}} \frac{1}{\mathcal{S}} \frac{\Gamma\left(\frac{3}{2}\right)\zeta\left(\frac{3}{2}\right)}{2\pi^2} \left(\frac{k_B T}{\mathcal{D}}\right)^{3/2}, \tag{4}$$

where $\omega_k = \mathcal{D}k^2$, spin-wave stiffness $\mathcal{D} = 2\mathcal{S}\mathcal{J}a^2$, lattice constant a, v_{ws} volume of the Wigner-Seitz cell, while $\Gamma(x)$ and $\zeta(x)$ are the gamma and Riemann zeta functions. The $T^{3/2}$ dependence is known as Bloch's law [23].

In the ferrimagnet YIG the total magnetization is made up by two oppositely aligned sublattices with slightly different temperature-dependent magnetizations. At low temperatures they are rigidly locked to an antiparallel configuration by the strong nearest-neighbor exchange. At energies $\hbar\omega_{\mathbf{k}}/k_B \lessapprox 30$ K YIG's magnon dispersion is known to be quadratic and its magnetization obeys Bloch's $T^{3/2}$ law [24]. The expected deviations at higher temperatures can be assessed by our method. We calculate the magnetization at temperature T as an average $\langle \cdots \rangle_T$ over the spin configurations at many times over a 1 ns trajectory $\mathbf{m}(T) = \langle N^{-1} \sum_i^N \mu_{s,i} \mathbf{S}_i \rangle_T / \langle N^{-1} \sum_i^N \mu_{s,i} \mathbf{S}_i \rangle_{T=0}$, where $N = 655\,360$ is the total number of spins in the simulation.

Figure 2 exposes the obvious problem of classical statistics to compute magnetizations at low temperatures: The magnetization decreases much more rapidly with temperature than Bloch's law (and as observed in experiments). The results with the quantum thermostat, on the other hand, adhere to Bloch's law for $T < 30$ K (see the inset) but also agree well with experiments that signal a breakdown of $T^{3/2}$ scaling, at least until ~300 K.

The Curie temperatures for the classical ($T_C = 420$ K) and quantum thermostated systems ($T_C = 680$ K) are quite different, while the observed $T_C = 550$ K lies between the theoretical values. In contrast to classical results that obey equipartition, the Curie temperature of quantum approaches depends on S and we find this also in our semiquantum approach. For a simple ferromagnetic bcc lattice our computed Curie temperatures agree well with those obtained by semianalytic approaches [25] for a large range of $\mathcal{S}$ (see Supplemental Fig. S3). The overestimation of T_C compared to the experiment might be caused by exchange parameters that are slightly too large since the neutron scattering data are fitted only up to 90 meV which does not cover the magnon modes with highest energy. Also, the choice of $\mathcal{S} = 5/2$ ($\mu_s = 5\mu_B$) in extracting the exchange parameters does not fully agree with the measured values of $\mu_{s,a} = 4.11\mu_B$ and $\mu_{s,d} = 5.37\mu_B$ for the octahedral and tetrahedral sites [26]. Hence, a more accurate set of parameters, fitted to neutron scattering data for large energy transfers or calculated from first principles, should solve this discrepancy.

Heat capacity. The magnon heat capacity per unit volume $C_m = V^{-1}(\partial U_m/\partial T)_V$ is the change in the internal magnetic energy U_m with temperature at constant volume V. It can be calculated from the magnon spectrum as $C_m = V^{-1}(\partial/\partial T) \sum_{\mathbf{k}\nu} \hbar\omega_{\mathbf{k}\nu} \langle n_{\mathbf{k}\nu} \rangle$, where $\langle n_{\mathbf{k}\nu} \rangle$ is the Planck distribution. In the low-temperature limit magnons occupy only states close to $k = 0$, where the magnon dispersion of ferromagnets is parabolic. For a single parabolic magnon band [13],

$$C_m(T) = \frac{1}{V} \frac{5}{8} \frac{\Gamma\left(\frac{5}{2}\right)\zeta\left(\frac{5}{2}\right)}{\pi^2} k_B \left(\frac{k_B T}{\mathcal{D}}\right)^{3/2}, \tag{5}$$

where $\Gamma(x)$ and $\zeta(x)$ are the gamma and Riemann zeta functions.

The proportionality $C_m \propto T^{3/2}$ should hold for YIG up to energies of $\hbar\omega_{\mathbf{k}}/k_B \lessapprox 30$ K. Rezende and López Ortiz [7] calculated the heat capacity for acoustic magnons with a finite bandwidth, but neglected optical magnons that contribute to the heat capacity at elevated temperatures. They found that C_m saturates at 150 K, i.e., when the magnon occupation reaches the upper band edge.

Here, we calculate the heat capacity including all magnon modes and their interactions. We calculate C_m from the energy fluctuations in the canonical ensemble $\langle U_m \rangle_T = (1/Z_m) \sum_{\mathbf{k}\nu} \hbar\omega_{\mathbf{k}\nu} \exp(-\hbar\omega_{\mathbf{k}\nu}/k_B T)$, where $Z_m = \sum_{\mathbf{k}\nu} \exp(-\hbar\omega_{\mathbf{k}\nu}/k_B T)$ is the partition function. Then $C_m = (\langle U_m^2 \rangle_T - \langle U_m \rangle_T^2)/(V k_B T^2)$, where in a simulation $\langle \cdots \rangle_T$ is an average over a large time interval at a constant temperature and V is the volume of the system.

Figure 3 shows the low-temperature region where the magnon dispersion is, to a good approximation, parabolic and $C_m \propto T^{3/2}$. Calculations using quantum statistics give an excellent agreement with Bloch's law. The experimental data in Fig. 3 have been collected in the range $T = 2$–9 K [5], high enough that dipolar field effects can be disregarded. The measurements were made by freezing the magnons in a 7-T field. Even this large field, however, does not completely remove the magnon contribution to the heat capacity, especially at the higher end of the temperature range [7]. To make a

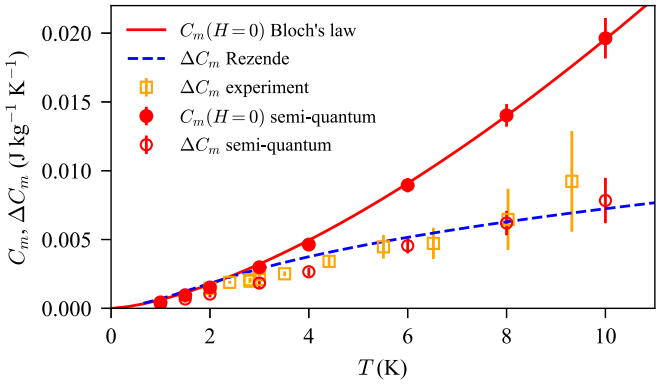

FIG. 3. Low-temperature magnon heat capacity of YIG calculated with quantum statistics (red circles) compared to Bloch's law (red solid line). $\Delta C_m = C_m(H = 0\ \mathrm{T}) - C_m(H = 7\ \mathrm{T})$ calculated with quantum statistics (red open circles) is compared with experimental data from Boona and Heremans [5] (orange open squares) as well as a single magnon band model [7] (blue dashed line). The error bars on simulated data represent three standard deviations across five independent stochastic trajectories.

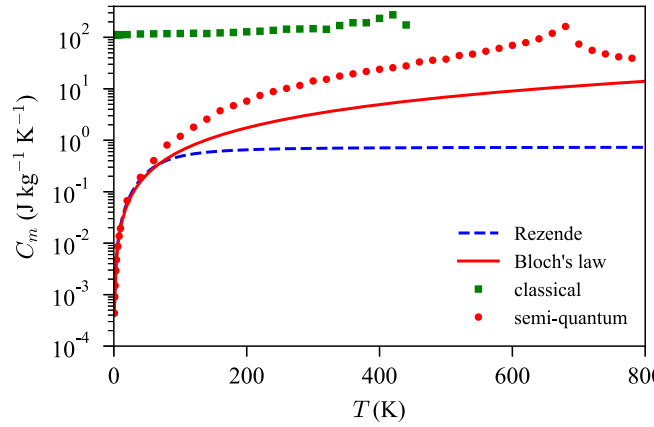

FIG. 4. YIG magnon heat capacity calculated over a larger temperature range with the semiquantum model (red circles), classical model (green squares), compared with Bloch's law (solid red line) and the single-band model [7] (dashed blue line).

proper comparison we repeat the experimental procedure in our simulation by computing the difference $\Delta C_m = C_m(H = 0\ \mathrm{T}) - C_m(H = 7\ \mathrm{T})$. Our calculations agree well with the observations as well as the single magnon-band model.

Figure 4 illustrates a pronounced difference between the classical and semiquantum models: Classical statistics overestimate the heat capacity by five orders of magnitude at low temperatures, and do not depend on temperature in contrast to the quantum statistical result which approaches zero as $T^{3/2}$. In spite of this spectacular (and rather obvious) failure, classical statistics have traditionally been used (and still are) in both Monte Carlo and atomistic spin dynamics.

At $T > 30$ K nonparabolicities begin and $C_m \propto T^p$ with power $p > 3/2$. At room temperatures Fig. 4 reveals differences between the approaches of two orders of magnitude. The finite-width magnon-band model [7] (dashed line in Fig. 4) saturates prematurely with increasing T because optical and higher acoustic modes become significantly occupied when approaching room temperature [9]. The parabolic band model without a high-momentum cutoff (Bloch's law) also strongly underestimates C_m because YIG's magnon density of states is strongly enhanced by the flat bands observed in Fig. 1. The semiquantum calculation is an order of magnitude larger than both of these heavily approximated approaches, benefitting from the complete description of the magnon spectrum as well as magnon-magnon interactions, while the classical statistics strongly overestimates the heat capacity up to the Curie temperature. Since the magnon heat capacity cannot be measured for $T > 10$ K, this is a critical test of the theories.

Conclusions. By enforcing Planck statistics for the magnons in the complex ferrimagnet YIG, we obtain excellent agreement with available inelastic neutron scattering and magnon heat capacity experiments. Our results prove that fundamental thermodynamic equilibrium properties can be predicted with confidence when experimental data are not available, but only when quantum statistics and the full spin-wave spectrum are taken into account. The method is not limited to YIG or ordered magnets, but can be directly applied to other complex materials with local magnetic moments such as spin glasses or paramagnets. Our results are a necessary step to compute nonequilibrium properties such as magnon conductivities and spin Seebeck coefficients, which are essential parameters for future applications of magnonic devices.

Acknowledgments. This work was supported by JSPS KAKENHI Grant No. 26103006, the Graduate Program in Spintronics (GP-Spin), Tohoku University, and MaHoJeRo (DAAD Spintronics network, Project No. 57334897). The authors thank Jiang Xiao, Yaroslav Tserkovnyak, Rembert Duine, and Jerome Jackson for valuable discussions.

[1] V. Cherepanov, I. Kolokolov, and V. L'vov, The saga of YIG: Spectra, thermodynamics, interaction and relaxation of magnons in a complex magnet, Phys. Rep. **229**, 81 (1993).

[2] *Recent Advances in Magnetic Insulators - From Spintronics to Microwave Applications*, edited by M. Wu and A. Hoffmann (Academic, New York, 2013).

[3] L. J. Cornelissen, J. Liu, R. A. Duine, J. B. Youssef, and B. J. van Wees, Long-distance transport of magnon spin information in a magnetic insulator at room temperature, Nat. Phys. **11**, 1022 (2015).

[4] L. J. Cornelissen, K. J. H. Peters, G. E. W. Bauer, R. A. Duine, and B. J. van Wees, Magnon spin transport driven by the magnon chemical potential in a magnetic insulator, Phys. Rev. B **94**, 014412 (2016).

[5] S. R. Boona and J. P. Heremans, Magnon thermal mean free path in yttrium iron garnet, Phys. Rev. B **90**, 064421 (2014).

[6] R. Douglass, Heat transport by spin waves in yttrium iron garnet, Phys. Rev. **129**, 1132 (1963).

[7] S. M. Rezende and J. C. López Ortiz, Thermal properties of magnons in yttrium iron garnet at elevated magnetic fields, Phys. Rev. B **91**, 104416 (2015).

[8] J. Oitmaa and T. Falk, Ferrimagnetism in the rare-earth iron garnets: A Monte Carlo study, J. Phys.: Condens. Matter **21**, 124212 (2009).

[9] J. Barker and G. E. W. Bauer, Thermal Spin Dynamics of Yttrium Iron Garnet, Phys. Rev. Lett. **117**, 217201 (2016).

[10] J. S. Plant, Spinwave dispersion curves for yttrium iron garnet, J. Phys. C **10**, 4805 (1977).

[11] A. J. Princep, R. A. Ewings, S. Ward, S. Tóth, C. Dubs, D. Prabhakaran, and A. T. Boothroyd, The full magnon spectrum of yttrium iron garnet, npj Quantum Mater. **2**, 63 (2017).

[12] We prefer the Landau-Lifshitz rather than the Gilbert damping, because latter affects the frequencies (here governed exclusively by the exchange parameters) by a factor $1/(1+\eta^2)$.

[13] C. Kittel, *Quantum Theory of Solids* (Wiley, New York, 1963).

[14] L. D. Landau and E. M. Lifshitz, *Statistical Physics*, 3rd ed. (Elsevier, Amsterdam, 1980).

[15] C. H. Woo, H. Wen, A. A. Semenov, S. L. Dudarev, and P.-W. Ma, Quantum heat bath for spin-lattice dynamics, Phys. Rev. B **91**, 104306 (2015).

[16] R. F. L. Evans, U. Atxitia, and R. W. Chantrell, Quantitative simulation of temperature-dependent magnetization dynamics and equilibrium properties of elemental ferromagnets, Phys. Rev. B **91**, 144425 (2015).

[17] H. Dammak, Y. Chalopin, M. Laroche, M. Hayoun, and J. J. Greffet, Quantum Thermal Bath for Molecular Dynamics Simulation, Phys. Rev. Lett. **103**, 190601 (2009).

[18] A. V. Savin, Y. A. Kosevich, and A. Cantarero, Semiquantum molecular dynamics simulation of thermal properties and heat transport in low-dimensional nanostructures, Phys. Rev. B **86**, 064305 (2012).

[19] U. Atxitia, O. Chubykalo-Fesenko, R. W. Chantrell, U. Nowak, and A. Rebei, Ultrafast Spin Dynamics: The Effect of Colored Noise, Phys. Rev. Lett. **102**, 057203 (2009).

[20] A. Rückriegel and P. Kopietz, Rayleigh-Jeans Condensation of Pumped Magnons in Thin-Film Ferromagnets, Phys. Rev. Lett. **115**, 157203 (2015).

[21] See Supplemental Material at http://link.aps.org/supplemental/10.1103/PhysRevB.100.140401 for technical details of the quantum thermostat and testing in a simple ferromagnetic system.

[22] M. D. Kuz'min, Shape of Temperature Dependence of Spontaneous Magnetization of Ferromagnets: Quantitative Analysis, Phys. Rev. Lett. **94**, 107204 (2005).

[23] F. Bloch, Zur theorie des ferromagnetismus, Z. Phys. **61**, 206 (1930).

[24] C. M. Srivastava and R. Aiyar, Spin wave stiffness constants in some ferrimagnetics, J. Phys. C **20**, 1119 (1987).

[25] J. Oitmaa and W. Zheng, Curie and Néel temperatures of quantum magnets, J. Phys.: Condens. Matter **16**, 8653 (2004).

[26] D. Rodic, M. Mitric, R. Tellgren, H. Rundlof, and A. Kremenovic, True magnetic structure of the ferrimagnetic garnet $Y_3Fe_5O_{12}$ and magnetic moments of iron ions, J. Magn. Magn. Mater. **191**, 137 (1999).

[27] E. E. Anderson, Molecular field model and the magnetization of YIG, Phys. Rev. **134**, A1581 (1964).